*ISSN 1392 - 1207. MECHANIKA. 2012 Volume 18(4): 398-402*

# Stress concentration at the shallow notches of the curved beams of circular cross-section

**E. Narvydas*, N. Puodžiūnienė****
**Kaunas University of Technology, Kęstučio 27, 44312 Kaunas, Lithuania, E-mail: Evaldas.Narvydas@ktu.lt*
***Kaunas University of Technology, Kęstučio 27, 44312 Kaunas, Lithuania, E-mail: Nomeda.Puodziuniene@ktu.lt*

crossref http://dx.doi.org/10.5755/j01.mech.18.4.2341

## 1. Introduction

The article continues to present the research work on the estimation of the circumferential stress ($\sigma_\Theta$) concentration factors ($K_{t\Theta}$) of the curved members effected by the asymmetric shallow notches. Previous publications [1, 2] were focused on calculations of the $K_{t\Theta}$ for the notched lifting hooks of trapezoidal cross-section. The present article assumes the curved beam of the circular gross cross-section under the transverse load. The method of the $K_{t\Theta}$ calculation is the same as in the previous article [2] therefore, will not be discussed here. However, the results will be presented for the additional 92 cases of different cross-section and notch geometry.

The article also includes results of the notch effect on a stress triaxiality under the elastic stress state with the evolution to the increasing elastic-plastic deformation. The stress triaxiality is known as an important factor for the failure prediction of the components.

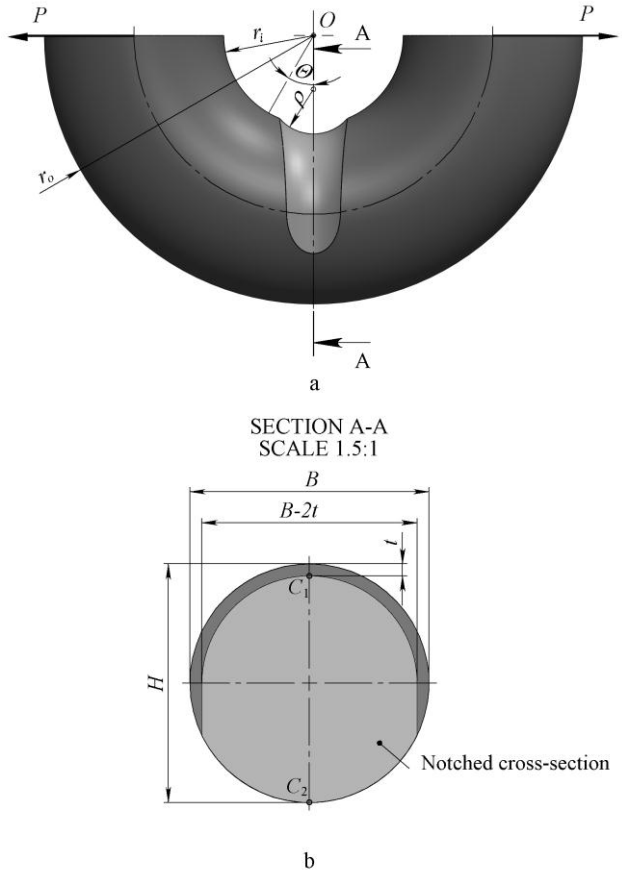


Fig. 1 Applied loading scheme and geometry of a notched lifting hook

The geometry of the curved beams is shown in the Fig. 1. Diameter of the circular gross cross section (a height of the cross-section $H$) was 100, 80 and 50 mm. The beam curvature was defined by ratio $r_c/H = 1.0$ for all cases. Here $r_c$ is a distance from the center of curvature to the geometrical center (centroid) of the cross-section.

The load ($P$) was applied at the ends of the curved beam with $\Theta = \pm 90°$ (Fig. 1). Therefore, the circumferential stresses $\sigma_\Theta$ were caused by the normal force $N = P$ and the bending moment $M_c = N\, r_c$.

## 2. Finite element models

As it was demonstrated earlier [2], the finite element analysis (FEA) is a suitable way to calculate both: the maximal circumferential stresses ($\sigma_{\Theta max}$) and the nominal circumferential stresses ($\sigma_{\Theta nom}$) needed to obtain the $K_{t\Theta}$. The finite element models were constructed employing symmetry boundary conditions (BC) that allowed to use 1/4 of the geometry. The point $C_2$ had an additional vertical motion restraint to complete the model's BC definition. The models were meshed with tetrahedral second order finite elements (element type SOLID187 of ANSYS™). The Fig. 2 shows the generic model for the $\sigma_{\Theta max}$ calculation.

The $\sigma_{\Theta max}$ were calculated at the notch root (point $C_1$ on the symmetry line of the notched cross section in Fig. 1). The $\sigma_{\Theta nom}$ were calculated at the same point, but in a curved beam of the consistent (uniform) cross section, i.e. the cross sections of the notched members at the notch root were equal to the cross sections of the members without a notch. Thus, the stress concentration effect

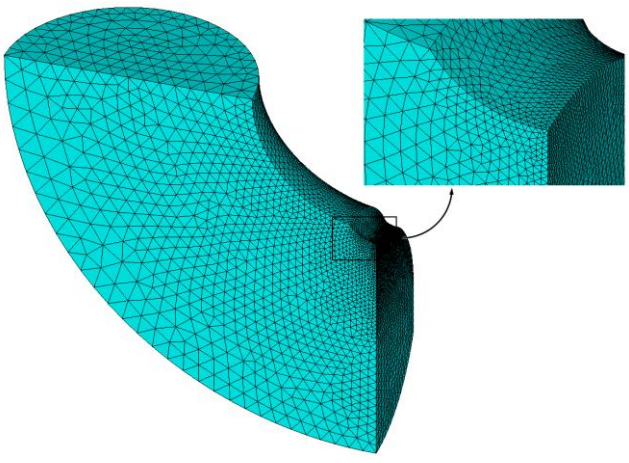

Fig. 2 Illustration of a generic 3D finite element model of a notched curved beam

caused by the notch was separated from the stress concentration caused by the curvature of the member or other factors.

Material properties were defined considering low carbon steel after the thermal normalization. Mechanical properties of this steel are presented in Table 1; only the Yong's modulus and Poison's ratio were used in the elastic stress analysis under quasi-static load.

Table 1

Mechanical properties of a low carbon steel

| Yong's modulus $E$, MPa | Poison's ratio $\nu$ | 0.2% proof strength $R_{p0.2}$, MPa | Tensile strength $R_m$, MPa | Elongation after fracture $A_5$, % | Reduction in cross section on fracture $Z$, % |
|---|---|---|---|---|---|
| 210000 | 0.29 | 245 | 412 | 25 | 55 |

## 3. Circumferential stress concentration factors and fitting curves

The results of $K_{t\Theta}$ for the curved beams of gross diameters ($H$) 100, 80 and 50 mm are presented in Figs. 3-5. The values of $K_{t\Theta}$ obtained by the FEA were used to find the fitting coefficients of Eqs. (1)-(3), similarly as in the earlier presented work [2]. The fitting Eqs. here are of two forms: general (1) with the three fitting coefficients and simplified with only the one fitting coefficient ((2) and (3)):

$$K_{t\Theta} = a\xi^{b}+c \text{ (general form)}, \quad (1)$$

$$K_{t\Theta} = 2\xi^{0.5}+c_f, \text{ if } 0.5 \le c_f \le 1.0 \quad (2)$$

$$K_{t\Theta} = (2\xi^{0.5}+0.5)\, d_f, \text{ if the fitted } c_f < 0.5 \text{ (Eq. (2))} \quad (3)$$

here $a$, $b$, $c$, $c_f$ and $d_f$ are the fitting coefficients; $d_f$ has values in a range from 0 to 1 and $c_f$ is in a range from 0.5 to 1.0. The $\xi$ is a geometry parameter $\xi = t/\rho$, where $t$ is a notch depth and $\rho$ is a notch root radius (Fig. 1).

Solid lines (Figs. 3 - 5) show the fitting results of Eq. (1). The dashed curves present the results of Eq. (2) and the dash-dot curves show the fitting results of Eq. (3). Because of the small difference between the results of Eq. (1) and Eq. (2), and similarly between Eq. (1) and Eq. (3), the corresponding curves look almost coincident in

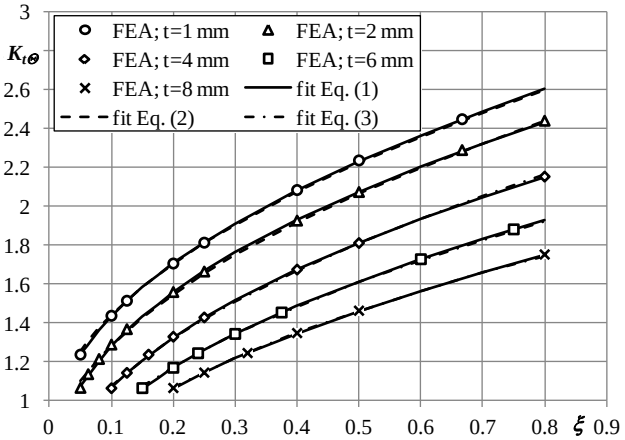


Fig. 3 Stress concentration factors $K_{t\Theta}$ for the curved beam of circular cross section ($H$ = 100 mm)

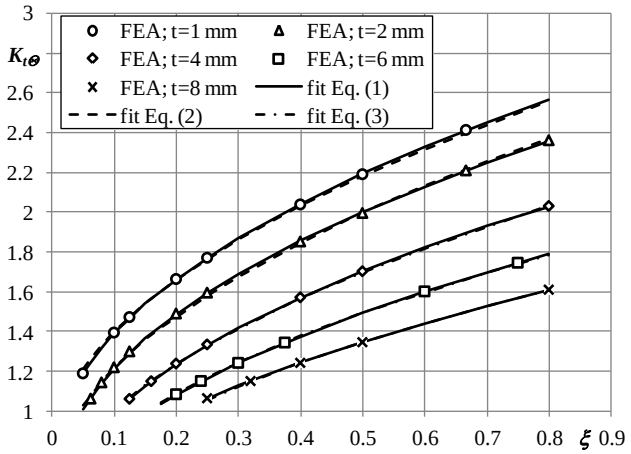


Fig. 4 Stress concentration factors $K_{t\Theta}$ for the curved beam of circular cross section ($H$ = 80 mm)

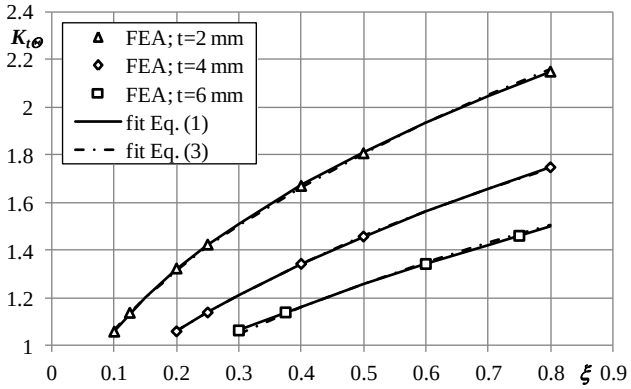


Fig. 5 Stress concentration factors $K_{t\Theta}$ for the curved beam of circular cross section ($H$ = 50 mm)

Figs. 3-5. The maximum relative difference of the $K_{t\Theta}$ calculated by Eq. (1) was less than 1% and by Eqs. (2) and (3) it was less than 3% comparing to the FEA results. The values of fitted coefficients $a$, $b$, $c$, $d_f$ and $c_f$ are presented in Table 2.

Table 2

Fitting data

| Geometry | | Fitted coefficients | | | | |
|---|---|---|---|---|---|---|
| $H$ | $t$ | Eq. (1) | | | Eqs. (2) and (3) | |
| | | $a$ | $b$ | $c$ | $c_f$ | $d_f$ |
| 100 | 1 | 2.09 | 0.466 | 0.716 | 0.806 | – |
| | 2 | 2.15 | 0.431 | 0.483 | 0.649 | – |
| | 4 | 2.00 | 0.437 | 0.331 | – | 0.944 |
| | 6 | 1.768 | 0.467 | 0.332 | – | 0.839 |
| | 8 | 1.512 | 0.515 | 0.401 | | 0.762 |
| 80 | 1 | 2.10 | 0.468 | 0.677 | 0.766 | – |
| | 2 | 2.11 | 0.435 | 0.437 | 0.582 | – |
| | 4 | 1.888 | 0.450 | 0.321 | – | 0.887 |
| | 6 | 1.570 | 0.506 | 0.387 | – | 0.779 |
| | 8 | 1.283 | 0.568 | 0.479 | – | 0.704 |
| 50 | 2 | 2.00 | 0.438 | 0.332 | – | 0.944 |
| | 4 | 1.508 | 0.517 | 0.405 | – | 0.762 |
| | 6 | 1.082 | 0.633 | 0.560 | – | 0.659 |

The final aim of this research was to find the universal relation that engineers could use for critical stress calculation. This relation should be simple and link the fitted coefficients $c_f$ and $d_f$ to some geometric characteristics of the component. As in the previous work, this characteristic was chosen to be a ratio $\eta = t/H$ and the relation to have a form of a second order polynomial. Fitted polynomial to the results of $c_f$ and $d_f$ from Table 2 versus the $\eta$ gave the following expressions:

$$c_f = 145.2\eta^2 - 20.1\eta + 0.994 \quad (4)$$

$$d_f = 25.0\eta^2 - 7.52\eta + 1.203 \quad (5)$$

Graphically the fitted polynomial curves are presented in Fig. 6 by continuous lines. The dotted lines present the earlier considered cases for lifting hooks of trapezoidal cross-section [2] for comparison. As it can be seen, the $c_f$ curves are not coincident, but close within relative difference not exceeding the 5%. The $d_f$ curves are close to each other within the same range of the relative difference, except when the $\eta > 0.08$. Therefore, the established relations are not universal, however still can be used as one for the evaluation of the $K_{t\Theta}$ with the acceptable error.

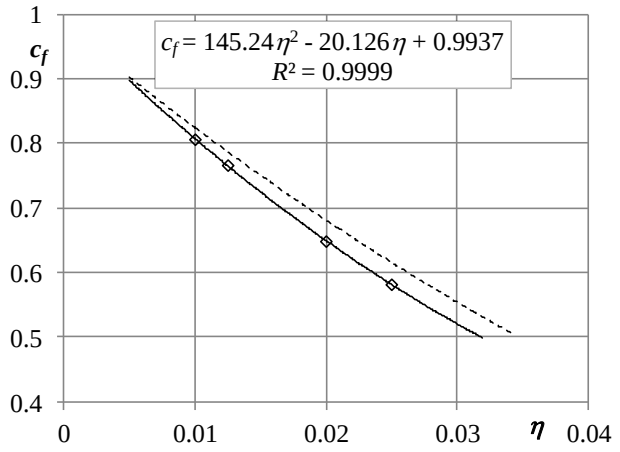


a

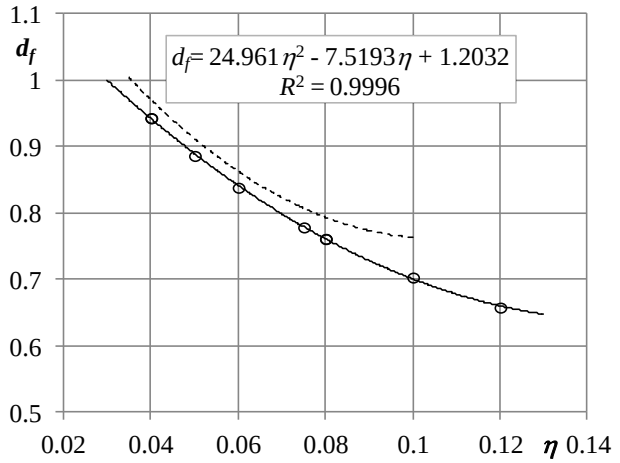


b

Fig. 6 Fitted coefficients $c_f$ (a) and $d_f$ (b) vs. geometric parameter $\eta$

## 4. Evolution of the stress triaxiality

The notch effects not only the circumferential stresses, but all components of the stress state, therefore, it effects the stress state multiaxiality. The stress multiaxiality causes the reduction of ductility of the material and influences the failure mode of the components. There are several approaches where this effect is accounted.

One approach, initially proposed by Davis and Connely [3], uses the stress triaxiality factor (*TF*), to account the stress multiaxiality effect in calculation of strain based failure criteria. It is used in cases where the accumulation of the plastic strains takes place: large quasistatic loads, creep, low cycle fatigue and impact. The expression of this factor is a ratio of the three times the hydrostatic pressure and the von Mises equivalent stress. Then the equivalent strain under the multiaxial stress state, or strain range in case of low cycle fatigue, is multiplied by multiaxiality factor *MF*, which is related to *TF* and equated to the uniaxial critical strain e. g. maximum uniform strain at uniaxial tension. For many practical cases [4] the research work of Manjoine [5] is addressed and *MF* is defined as follows:

$$MF = TF, \text{ if } TF \le 2 \quad (6)$$

and

$$MF = 2^{TF-1}, \text{ if } TF > 2 \quad (7)$$

Some sources prefer the identical expression $MF = 1/2^{1-TF}$; it is also often assumed to use $MF = 1$, if $TF < 1$ [4, 6].

The *TF* values usually are calculated as an average through the wall thickness (for vessels) [6] or through the cross section (for beams) under the elastic stress state. The possible change of *TF* under the increasing plastic strain is disregarded.

In case of low cycle fatigue, when cyclic plastic strain range is used for lifetime (number of cycles) calculation, the basic expressions of *MF* are [7]

$$MF = 1/(2 - TF), \text{ if } TF \le 1 \quad (8)$$

and

$$MF = TF, \text{ if } TF > 1 \quad (9)$$

If the energy-based approach is used [8], for the cyclic plastic work

$$MF = 2^{k_1(TF_S - 1)} \quad (10)$$

and for the effective elastic distortion strain energy parameter to account the mean stress effect in case of non-symmetric cycle

$$MF = 2^{k_2 TF_m} \quad (11)$$

here $TF_S$ and $TF_m$ are the stress triaxiality factors calculated using amplitudes *S* and mean values *m* of the principal cyclic stresses; $k_1$ and $k_2$ are the calibration constants.

The continuum damage mechanics approach, [9-11] uses the stress triaxiality parameter $T_x = \sigma_H / \sigma_{eq}$ (ra-

tio of hydrostatic and equivalent von Mises stresses) and the stress triaxiality function

$$R_\nu = 2/3(1+\nu)+3(1-2\nu)(\sigma_H/\sigma_{eq})^2 \quad (12)$$

Relation of the equivalent accumulated plastic strain ($p$) under multiaxial stress state can express the influence of stress triaxiality on ductility reduction [10, 11]

$$p = \varepsilon_{th}\left(\varepsilon_f / \varepsilon_{th}\right)^{1/R_\nu} \quad (13)$$

where $\varepsilon_{th}$ and $\varepsilon_f$ are damage strain threshold and failure strain under uniaxial stress state of the material. The one could notice that under the uniaxial stress state the $R_\nu = TF = 1$ and the difference between $T_x$ and $TF$ is in a constant factor of 3.

To see the shallow notch effect on the stress triaxiality factor, the $TF$ values along the symmetry line of the cross section of the smooth and notched ($H$ = 80 mm, $t$ = 4 mm, $\rho$ = 10 mm) curved beams were calculated. Because the stress triaxiality effects failure only when the plastic straining take place, the nonlinear FEA was performed using bilinear uniaxial stress strain curve approximation with yield stress point 245 MPa (Table 1) and the tangent modulus $E_T$ = 671 MPa. The $TF$ values were calculated over the cross section under the several load levels and elastic plastic straining. Figs. 7 and 8 show the equivalent plastic strains ($\varepsilon_{pleq}$, curves *1*, *2*, *3*) and $TF$ values (curves *1′*, *2′*, *3′*) for smooth and notched curved beam on the part of the symmetry line of the cross section under the dominating tensile normal stresses and positive $TF$ values. The corresponding load levels were: $P$ = 72 kN (curves *1* and *1′*), $P$ = 130 kN (curves *2* and *2′*) and $P$ = = 160 kN (curves *3* and *3′*). The maximum equivalent plastic strains under these load levels for the smooth beam were: 0.0017, 0.139 and 0.362; for notched beam: 0.00482, 0.0365 and 0.423. The dotted curves 0′ represent the $TF$ under the elastic stress state.

The results of $TF$ demonstrate the local increase of the triaxiality at the initial stage of plastic straining comparing to the elastic stress state (curves *1′*, Figs. 7 and 8). Then, under the growing load and plastic straining, the $TF$ further increases at the large zone of the cross section, but slightly decreases at the inner surface of a beam curvature (curves *2′*). Under the further development of the load, when the plastic strain zone covers the entire cross section, the $TF$ values are decreasing and are getting lower comparing to the ones under the elastic stress state (curves *3′*). This behavior is characteristic for both, the smooth and the notched curved beams, but the local increase of $TF$ is more sharply expressed in the notched beam (curves *1′*) and the overall values of $TF$ are higher in the notched beam. These results allow to conclude, that the stress triaxiality factors at the load levels near the failure are lower comparing to the ones under the elastic stress state. Assuming that the stress multiaxiality effects the failure strain only at the final (failure) stage of the straining, the usage of $TF$ calculated under the elastic stress state would be conservative. However, if the assumptions of the continuum damage mechanics would be used, then the damage accumulation would take place under the changing stress triaxiality during the development of the equivalent strain starting from the threshold strain ($\varepsilon_{th}$). Depending on the materials

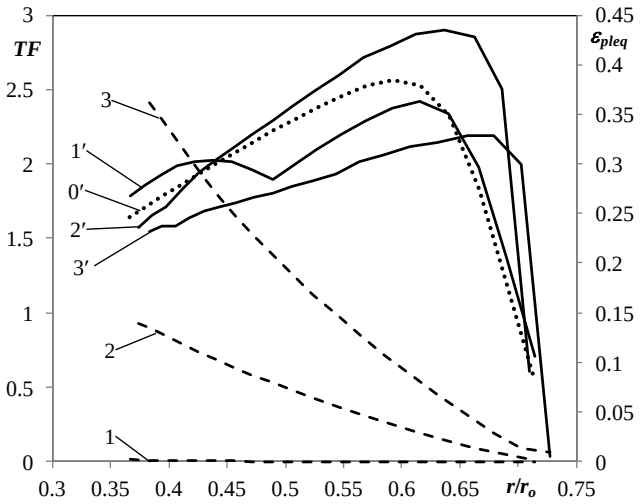


Fig. 7 Evolution of the equivalent plastic strain and the stress triaxiality factor of the smooth curved beam ($H$ = 80 mm; $t$ = 4 mm)

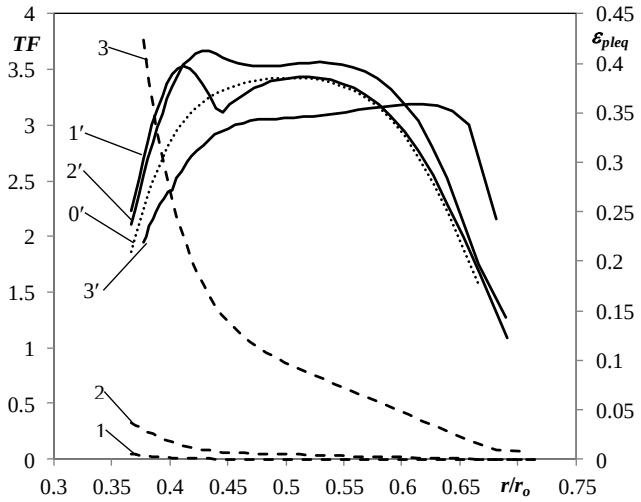


Fig. 8 Evolution of the equivalent plastic strain and the stress triaxiality factor of the notched curved beam ($H$ = 80 mm; $t$ = 4 mm; $\rho$ = 10 mm)

$\varepsilon_{th}$, the damage accumulation range may cover the part of the plastic straining at the higher triaxiality then under the elastic stress state for the curved beams.

## 6. Conclusions

The single parameter depending on the geometry of the curved beams of circular cross-section with asymmetric shallow notches was found by fitting the selected equations to the FEA results. Comparing this parameter to the previously found parameters for the curved beam of trapezoidal cross-section allow to conclude that the established equations are acceptable for both cross-sections within the relative difference of 5%, except for the cases of $d_f$ where $\eta > 0.8$.

The evolution of the stress triaxiality factor under the large plastic straining demonstrates the increase of $TF$ at the beginning of the plastic straining and decrease at the later stage of loading for both smooth and notched curved beams. The decrease of the $TF$ under the large loads indicates that the use a $TF$ factor calculated under the elastic stress state is conservative if the Manjoine [5] assumption

is applied. However, if the assumptions of the continuum damage mechanics will be used, the approach to employ the $T_x$ calculated under the elastic stress state may be non-conservative, because the significant increase of *TF* (and $T_x$) was observed during the loading history. Therefore, the damage evolution should be considered starting from the threshold plastic strain and the increase of the $T_x$ should be accounted.

**References**


1. **Narvydas, E.** 2010. Modeling of a crane hook wear and stress analysis. Transport Means 2010: Proceedings of the 14th international conference; 2010 Oct 21-22; Kaunas University of Technology, Lithuania. Kaunas: Technologija. 161-164.
2. **Narvydas, E.; Puodžiūnienė, N.** 2012. Circumferential stress concentration factors at the asymmetric shallow notches of the lifting hooks of trapezoidal cross-section, Mechanika 18(2): 152-157. http://dx.doi.org/10.5755/j01.mech.18.2.1574.
3. **Davis, E.A.; Connelly, F.M.** 1959. Stress distribution and plastic deformation in rotating cylinders of strain-hardening material, Journal of Applied Mechanics-Transactions of the ASME 26: 25-30.
4. **Flanders, H.E**. 1995. Strain Limit Criteria to Predict Failure. Proceedings of the 5th DOE Natural Phenomena Hazard Mitigation symposium; 1995 November 13-17; Denver, Colorado. 164-168.
5. **Manjoine, M.J.** 1982. Creep-rupture behavior of weldments, Welding Journal 61: 50–57.
6. **Snow, S.D.; Morton, D.K.; Pleins, E.L.; Keating, R.** 2010. Strain-based acceptance criteria for energy-limited events. ASME Pressure Vessels and Piping Conference, Vol. 7: Operations, Applications and Components. 91-96.
7. **Manson, S.S.; Halford, G.R.** 1977. Discussion, Multiaxial low cycle fatigue of type 304 stainless steel, ASME Journal of Engineering Materials and Technology 99: 283-286.
8. **Park, J.; Nelson, D.** 2000. Evaluation of an energy-based approach and a critical plane approach for predicting constant amplitude multiaxial fatigue life, International Journal of Fatigue 22: 23-39. http://dx.doi.org/10.1016/S0142-1123(99)00111-5.
9. **Lemaitre, J; Desmorat, R.** 2005. Engineering Damage Mechanics: Ductile, Creep, Fatigue and Brittle Failures. Berlin: Springer. 380 p.
10. **Bonora, N.** 1997. A nonlinear CDM model for ductile failure, Engineering Fracture Mechanics 58:11-28. http://dx.doi.org/10.1016/S0013-7944(97)00074-X.
11. **Bonora N.; Ruggiero, A.; Esposito, L.; Gentile, D.** 2006. CDM modeling of ductile failure in ferritic steels: assessment of the geometry transferability of model parameters, International Journal of Plasticity 22: 2015–2047. http://dx.doi.org/10.1016/j.ijplas.2006.03.013.


E. Narvydas, N. Puodžiūnienė

ĮTEMPIŲ KONCENTRACIJA TIES NEGILIAIS GRIOVELIAIS KREIVUOSE APVALAUS SKERSPJŪVIO STRYPUOSE

R e z i u m ė

Straipsnyje nagrinėjama įtempių koncentracija apvalaus skerspjūvio kreivuose strypuose ties vidinėje išlenkimo pusėje esančio griovelio dugnu. Šis tyrimas papildo anksčiau išnagrinėto trapecinio profilio strypų atvejus ir leidžia spręsti apie sudarytų formulių tinkamumą ir universalumą.

Straipsnyje taip pat nagrinėjamas įtempių būvio erdviškumo ir plastinių deformacijų kitimas didinant apkrovą. Nustatyta, kad įtempių būvio erdviškumas prasidėjus strypo plastinėms deformacijoms yra didesnis lyginant su tampraus įtempių būvio atveju, tačiau, plastinėms deformacijoms apėmus visą strypo skerspjūvį, įtempių būvio erdviškumas sumažėja.

E. Narvydas, N. Puodžiūnienė

STRESS CONCENTRATION AT THE SHALLOW NOTCHES OF THE CURVED BEAMS OF CIRCULAR CROSS-SECTION

S u m m a r y

Paper presents the results of investigation of the stress concentration at the groves of the inner side of curvature for the curved beams of circular cross-section. This investigation supplements the earlier work for curved beams of trapezoidal cross-section and enables the evaluation of the suitability and versatility of the established equations for the calculation of the stress concentration factors.

The paper also presents the investigation results of the evolution of stress triaxiality and plastic strain under the increasing load. It was found that the stress triaxiality factor is higher at the beginning of the plastic deformation comparing to one calculated under the elastic stress state. However, when the plastic strain covers the entire cross section of the beam the stress triaxiality reduces.

**Keywords:** curved beams, stress concentration factors, stress triaxiality, FEA.

Received June 07, 2011
Accepted August 21, 2012